Available online at www.sciencedirect.com

ScienceDirect

Ceramics International 39 (2013) 9137–9144

CERAMICS INTERNATIONAL

www.elsevier.com/locate/ceramint

Sintering and crystallization of plates prepared from coarse glass ceramic frits

Jorge Henrique Piva[a], Augusto Wanderlind[b], Jeanini Just[b], Oscar Rubem Klegues Montedo[a,b,*], Agenor De Noni Junior[a,b]

[a]*Programa de Pós-Graduação em Ciência e Engenharia de Materiais (PPGCEM), Universidade do Extremo Sul Catarinense (UNESC), Av. Universitária 1105, 88806-000 Criciúma, Brazil*

[b]*Instituto de Engenharia e Tecnologia (IDT-UNESC), Universidade do Extremo Sul Catarinense (UNESC), Av. Universitária 1105, 88806-000 Criciúma, SC, Brazil*

Received 12 April 2013; received in revised form 2 May 2013; accepted 3 May 2013
Available online 13 May 2013

Abstract

The focus of this study was the development of a CAS glass-ceramic ($14.0CaO \cdot 5.5Al_2O_3.80 \cdot 5SiO_2$) for use in civil engineering as a decorative material. This glass-ceramic system was chosen because it can be used to produce plates with a similar appearance to those of marble and granite materials. Ceramic plates were produced by the Grain Glass Sintering process from frits with a coarse grain size (2.1 mm average particle size). Powder frit samples (5.3-μm average particle size) were prepared and characterized. The results were compared with those obtained with coarse particles. Thermal treatment was performed in one stage, with the heating rate varying from 2 to 25 °C min^{-1}. Temperatures were defined by differential thermal analysis and heating microscopy. With these results, it was possible to establish correlations among the esthetic effects, the microstructure, and the heat treatment conditions (temperature, heating rate, and holding time). The relative density ranged from 0.92 to 0.96. The formation of wollastonite and pseudowollastonite was observed. An esthetic effect similar to that of natural marble was more apparent in those samples in which the microstructure presented a visual contrast between the bulk and the coarse frit. Lower heating rates intensified the visual contrast and reduced porosity near the surface regions.

Keywords: A. Sintering; B. Microstructure-final; D. Glass ceramics; E. Structural applications

1. Introduction

Ceramics are an important alternative for use as decorative building materials. This class of materials combines technical performance, ease of cleaning, and esthetic characteristics that are compatible with current demands. Ceramic tiles are produced in large-scale plants by a well-known powder technology that includes uniaxial pressing, drying, decorating, and firing in roller kilns [1]. In recent years, this approach has been used to produce relatively large porcelain stoneware tiles measuring up to 1 m^2, such as plates that measure approximately 1.2 m × 1.2 m and are between 6 mm and 10 mm thick.

The current interest in the development of ceramic products is driving research on materials and manufacturing processes that share technical performance (mechanical strength, scratch hardness, and stain hardness among others) and esthetic characteristics (visual and dimensional aspects). Certain commercial products, such as Laminum™ [2] or the well-known Neoparies™ [3], are examples of products in this category. The Laminum products are porcelain stoneware tiles with areas of up to 3 m^2 and thicknesses of between 3 and 6 mm. These tiles are produced by powder pressing on a continuous belt. The Neoparies product line of glass-ceramic materials, with surface area up to 2 m^2 and thickness up to 15 mm, is obtained by sintering coarse grain frit in a refractory mold. Glass-ceramic plates, obtained by powder pressing followed by sintering and crystallization, are also suggested in the literature

*Corresponding author at: Instituto de Engenharia e Tecnologia (IDT-UNESC), Universidade do Extremo Sul Catarinense (UNESC), Av. Universitária 1105, 88806-000, Criciúma SC, Brazil. Tel.: +55 48 34312 775; fax: +55 48 3431 2650.

E-mail addresses: okm@unesc.net, oscar.rkm@gmail.com (O.R.K. Montedo).

0272-8842/$ - see front matter © 2013 Elsevier Ltd and Techna Group S.r.l. All rights reserved.
http://dx.doi.org/10.1016/j.ceramint.2013.05.011

as a potential option for making ceramic tiles with enhanced properties [4–6]. Other authors [7] suggest a process known as *cracked glass crystallization* (*CGC*) to produce glass-ceramic products with *pseudo-bioclassic texture* similar to that of ornamental stones.

The choice of the material and the processing route will depend on the desired technical and aesthetical characteristics of the product. The wollastonite-based glass-ceramic has been proposed as an alternative similar to marbles [7–9]. Thus, sintering coarse frits packed in refractory molds, also known as *Grain Glass Sintering* (*GGS*), is a technique for making products with the esthetic effect of marble. Large thick plates that resemble ornamental rocks may be produced easily. The literature also shows that this route may be used successfully to transform industrial waste into materials for architectural use with high aggregate value [10].

However, the use of this GGS manufacturing route is limited, and only a few studies have been published. Sintering of glass-ceramics by powder technology is widespread, and sintering and crystallization mechanisms are well-known [11,12]. Although sintering and crystallization phenomena are concurrent in most cases, there is interest in maximizing the performance of both phenomena [13].

The aim goal of this study is to investigate the sintering and the crystallization of a CAS glass-ceramic ($CaO–Al_2O_3–SiO_2$) obtained by the *GGS* process. We correlate the esthetic effect with the results obtained from thermal characterization of this ceramic. In addition to the technical attributes, we seek to reproduce an esthetic effect similar to that of marble products. This esthetic effect corresponds to opaque particles surrounded by the vitreous matrix with a translucent texture. The use of coarse frits with a surface crystallization mechanism might fulfill this requirement [11]. However, sintering and crystallization phenomena could not be limited by the particle sizes in the frits, considering the desired esthetic effects.

2. Materials and methods

2.1. Preparation of the frit

For this study, a composition belonging to the CAS system ($14.0CaO \cdot 5.5Al_2O_3 \cdot 80.5SiO_2$) was chosen. The selection criterion was based on the ability of the frit to crystallize in the wollastonite crystalline phase ($CaSiO_3$). Raw materials were mixed properly, placed in an alumina crucible, and melted at 1500 °C for 1 h in a bottom loading kiln (Jung model LF0916, Blumenau, Brazil). The frit was obtained by pouring the melted mixture into water at room temperature. Table 1 shows the chemical composition of the frit, which was determined by X-ray fluorescence (XRF, Philips PW 2400, Eindhoven, The Netherlands). The calcium oxide level was below the values used in previous studies [7,14], but the content of this frit was still within the desired limits. From this frit, two types of samples were produced: (1) PF, powder frit with d_{50}=5.3 μm (measured with a laser scattering particle size analyzer, Cilas 1064L, Orleans, France), and (2) CF, coarse frit with d_{50}=2.1 mm (determined by sieving). Fig. 1 shows the particle size distribution of these frits.

Table 1
Chemical composition of the used frit.

Oxides	SiO_2	Al_2O_3	K_2O	Na_2O	MgO	CaO	ZnO	BaO
wt%	63.56	7.42	2.12	3.50	0.21	10.28	5.19	7.72

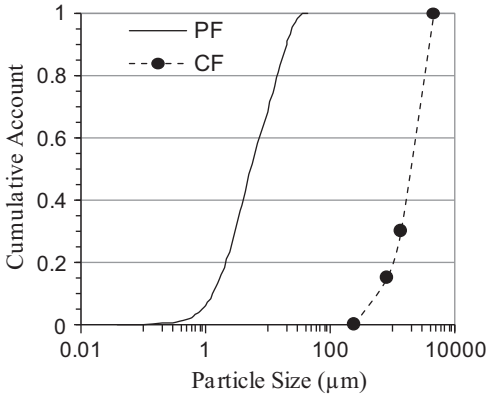

Fig. 1. Particle size distribution of the frits.

2.2. Thermal characterization

The temperatures of the glass transition (T_g) as well as the onset of crystallization (T_c) were determined by a high-temperature thermo analyzer (DTA, STA 409 EP, Netzsch, Selb, Germany; 10 °C min^{-1} heating rate, dry air). The temperatures for the maximum sintering rate and at the start of melting were evaluated by heating microscopy measurements (Misura® HSM ODHT 1400, Modena, Italy; 10 °C min^{-1} heating rate, air). In both cases, the powder frit (PF) was used according to typical procedures from glass-ceramics studies [4,15].

2.3. Preparation of specimens and experimental procedure

The specimens were produced by pouring CF and PF into a cylindrical mullite mold (40 mm diameter, 40 mm height) over a cordierite plate of 10 mm thickness, (A) and (B) in Fig. 2, respectively. The internal walls of the molds were coated with a thin layer of refractory magnetite-based engobe (C) that was applied by slip casting. The PF and the CF frits were put into the mold by slip casting (80 wt% solid content) and dry casting, respectively. In each mold, 40 g of frit (dry basis) was used. After the molds were filled, the frits were dried in a stationary laboratory dryer at 80 °C for 24 h.

The experimental procedure for firing consisted of two stages. First, specimens were fired at five temperatures. The heating rate was 10 °C min^{-1}, and the holding time at the maximum temperature was 120 min. The second stage was performed only with the CF frit, and the best temperature was

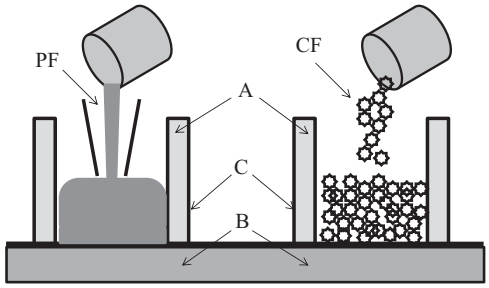

Fig. 2. Illustration of the mullite cylindrical mold (A), the cordierite plate (B), and the refractory engobe and (C) for frits PF and CF.

Table 2
Description of the experimental runs.

Run	T (°C)	Heating rate (°C min^{-1})	Holding time (min)	Frit
1	790	10	120	PF, CF
2	850	10	120	PF, CF
3	925	10	120	PF, CF
4	1000	10	120	PF, CF
5	1100	10	120	PF, CF
6	1145	10	120	PF, CF
7	1000	10	360	CF
8	1000	2	120	CF
9	1000	2	360	CF
10	1000	25	120	CF
11	1000	25	360	CF

defined during the first stage. Three heating rates and two maximum temperature levels were used. Table 2 shows the experimental conditions used in this study.

After firing, the apparent density of each specimen was determined by immersion in water (Archimedes' principle) at 20 °C. Theoretical densities of specimen powders, obtained by dry grinding in a tungsten carbide mill, were measured by He picnometry (Micromeritics Accupyc 1340, Norcross, USA), while crystalline phases were determined by X-ray diffractometry (Shimadzu XRD-6000, Kyoto, Japan; $2\theta = 10$–80°, 2 deg min^{-1}, Cu Kα1 radiation). After the heat treatment, each sample was cut transversally to evaluate its microstructure by optical microscopy (Olympus UC 30, Tokyo, Japan). Ten images of each specimen were taken, and the pore size distribution was quantified (Digimizer software version 4.2.2.0). This quantification was performed in two regions: near the particle surfaces and in the bulk matrix.

3. Results and discussion

3.1. Thermal characterization of the frit

Fig. 1 shows the thermal characterization results for the frit. From the linear thermal shrinkage plot ($\Delta L/L_o$ vs. T), the maximum sintering rate temperature (T_s) was approximately 790 °C, and the temperature at the start of melting (T_m) was estimated to be approximately 1025 °C. From the DTA plot, the temperatures of the glass transition (T_g) and at the start of crystallization (T_x) were estimated to be approximately

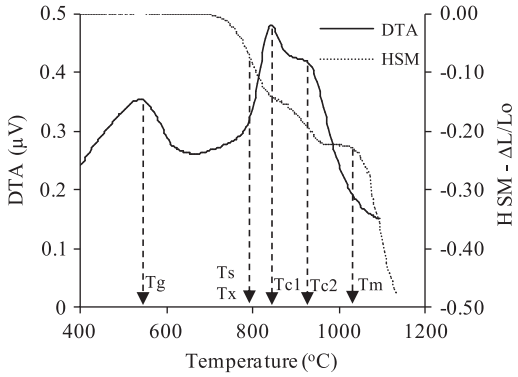

Fig. 3. DTA plot and linear thermal shrinkage of the frit PF indicating: the glass transition temperature (T_g), the temperature of the maximum sintering rate (T_s), the temperature at the start of crystallization (T_x), the temperatures at the onset of crystallization (T_{c1} and T_{c2}), and the temperature at the start of melting (T_m).

540 and 790 °C, respectively. The $T_x - T_s$ difference indicates the interdependence of the sintering and the crystallization phenomena, i.e., greater values of $T_x - T_s$ correspond to less interdependence [16,17]. In this study, the $T_x - T_s$ difference equals zero, which indicates that it was difficult for the investigated composition to achieve high levels of densification. Moreover, the DTA plot depicts two onsets of crystallization: T_{c1} at approximately 850 °C and T_{c2} at approximately 925 °C.

The material begins to shrink at approximately 720 °C and reaches its maximum sintering rate at 790 °C. This temperature closely agrees with the temperature at the start of crystallization. In fact, as already discussed in previous studies [15,16], the sintering rate is reduced to almost zero at the onset of crystallization.

There are many ways to determine the dominant mechanism of glass crystallization. Zanotto [18] and James and Jones [19] proposed evaluating the mechanism of crystallization in glasses from the T_g/T_m ratio. According to those authors, the crystallization mechanism is volumetric when the T_g/T_m ratio is < 0.58 and superficial or mixed when the T_g/T_m ratio is > 0.58. For the T_g and T_m values obtained for the frit in this work, the T_g/T_m value was 0.63, indicating crystallization by a superficial or mixed mechanism.

3.2. Effect of firing temperature on sintering

Fig. 4 presents the relative density as a function of temperature for the frits. For the frit PF, the maximum relative density, 0.91, was obtained at the temperature of the maximum sintering rate. As the firing temperature increased, the relative density decreased due to interference caused by crystallization upon sintering, i.e., $T_s \cong T_x$. Similar results were reported by other authors who studied wollastonite glass-ceramics with different frit particle size distributions [14] and observed the reduction of the relative density with increasing temperature for powders with smaller particles ($d_{50} = 2$ μm) [20].

The frit CF exhibited a lower relative density than the frit PF in the temperature range of the maximum sintering rate

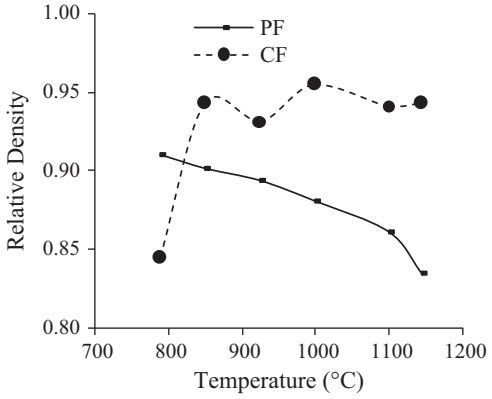

Fig. 4. Relative density as a function of temperature for frits PF and CF.

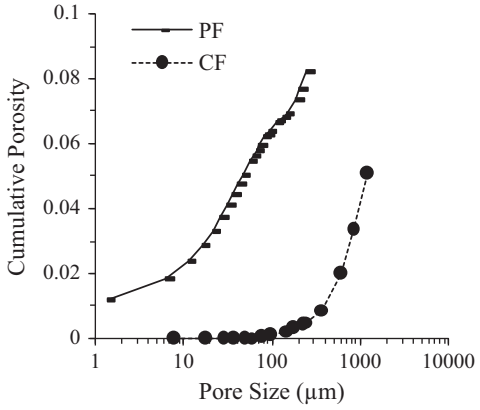

Fig. 5. Pore sizes distributions of frits PF and CF heat treated at 790 and 1000 °C, respectively.

because the frit CF contained coarser particles than the frit PF. This result is in agreement with the model proposed by Prado and Zanotto [13], where the increase in particle size reduces the sintering rate. However, we observed that the specimens reached relative densities between 0.93 and 0.96 above 850 °C, and the maximum values were achieved at 1000 °C. In this case, the reduction of surface area with increasing temperature should have significantly reduced the crystallization rate. Thus, this phenomenon should have reduced the negative effect on sintering and allowed the relative density to increase.

Fig. 5 shows the accumulated porosity as a function of pore diameter in the cross-section of the specimens at 790 and 1000 °C. As for the relative density, the porosity was higher for frit PF than frit CF. Measurements of the porosity obtained by image analysis were in good agreement with the relative density values. The average pore diameter (d_{50}) was≅30 μm and≅700 μm for frits PF and CF, respectively.

3.3. Effect of firing temperature on crystallization

Fig. 6 shows the XRD patterns for the frits heat treated at 1000 °C. The diffraction peaks corresponding to pseudowollastonite (α-$CaSiO_3$) and wollastonite are present for both frits PF and CF. However, the pseudowollastonite peaks are more pronounced for frit PF, and the wollastonite peaks are stronger for frit CF. The temperature effect on the peaks intensity in the crystallographic plane QUOTE ($2\theta=27.5^\circ$) related to pseudowollastonite and in the plane (320) ($2\theta=30^\circ$) related to wollastonite is shown in Fig. 7 for frit PF and frit CF. The formation of pseudowollastonite for frit PF begins at 850 °C, corresponding to the onset of the first crystallization peak in the DTA plot (Fig. 3). A significant increase in the peak intensity for wollastonite at 925 °C is visible. This temperature is in agreement with the onset of the second crystallization peak in the DTA plot (Fig. 3). At 1100 °C, the peak intensity of the pseudowollastonite decreased, most likely due to the solubilization of this crystalline phase in the glassy matrix. However, the peak intensity of the crystalline phase increased again at 1145 °C due to the polymorphic conversion of wollastonite to pseudowollastonite that occurs approximately 1127 °C [21,22]. The wollastonite formation approximately 925 °C and the

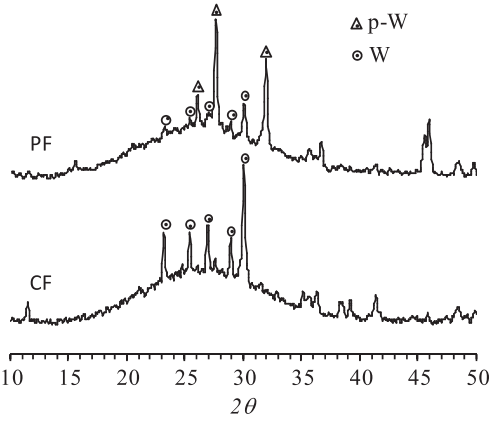

Fig. 6. XRD patterns of samples heat treated at 1000 °C. W: wollastonite and p-W: pseudowollastonite.

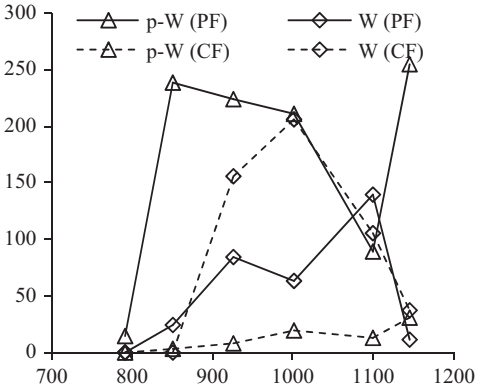

Fig. 7. Intensity of the XRD peaks for the crystallographic planes (320) ($2\theta=30^\circ$) of wollastonite (W) and ($23\bar{1}$) ($2\theta=27.5^\circ$) of pseudowollastonite (p-W).

polymorphic transformation approximately 1125 °C were reported in recent studies [7–9,23–26]. However, the early formation of pseudowollastonite at 850 °C is an interesting observation. According to the literature, the crystallization of wollastonite is affected strongly by the presence of impurities that act as mineralizing agents [9,24,25]. In this study, the reduction in

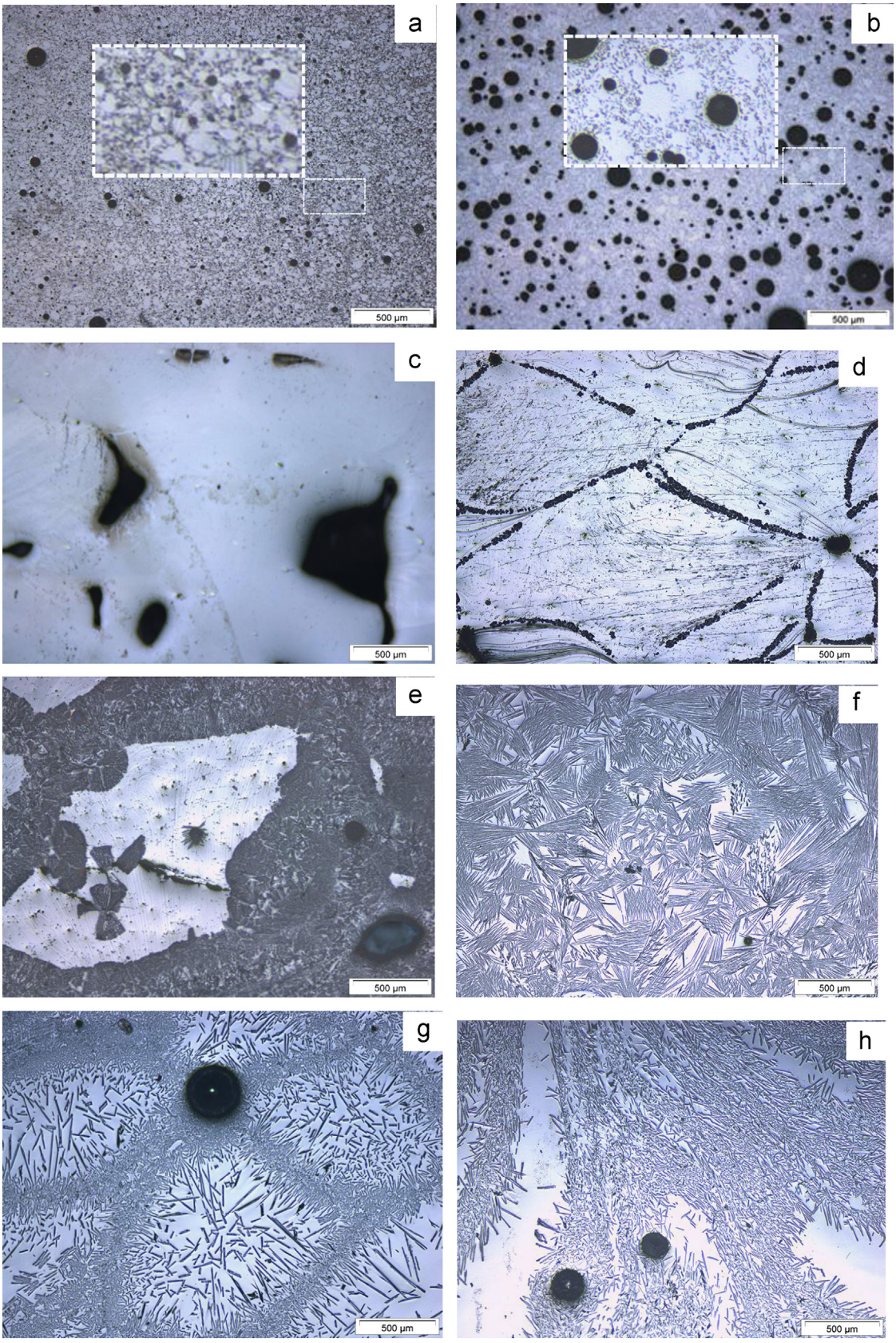

Fig. 8. Micrographs of the samples heat treated at PF (a) 790 and (b) 1145 °C; CF (c) 790, (d) 850, (e) 925, (f) 1000, (g) 1100 and (h) 1145 °C.

particle size most likely enhanced the ability of certain glass constituents to enhance the formation of pseudowollastonite.

For frit CF, wollastonite crystallized at 925 °C, as shown in the DTA plot. The maximum peak intensity occurred at 1000 °C. This result was expected because the viscosity of the liquid phase was lower at 1000 °C, providing better conditions for crystal growth [12]. As observed for frit PF, the peak intensity for frit CF decreased from 1100 °C with the onset of fusion, which was identified in the heating microscopy plot (Fig. 3). At 1145 °C, a polymorphic transformation of the small remaining amount of wollastonite occurred, resulting in a small increase in the pseudowollastonite peak.

Fig. 8 shows, the microstructure of frit PF at 790 and 1145 °C and of frit CF at all investigated temperatures. For frit PF, more and larger pores are observed with increasing temperature, which is in good agreement with the relative density results. A crystalline phase is present at the boundaries of both frits. Incipient crystallization can be considered at 790 °C, at the same temperature as at the higher sintering rate. In the case of frit CF at 790 °C, the pores are large and irregular, and no crystallization is apparent. At 850 °C, the size and the number of pores are significantly smaller. Intergranular pores were present, as well as intragranular pores that were generated during the frit preparation process. Incipient surface crystallization is visible at the boundaries of the frits. At 925 °C, the crystallization is present in the boundaries. Crystallization is also present around the intragranular pores. At 1000 °C, wollastonite crystals grow along the entire evaluated region. However, surface crystallization is not evident because it is more difficult to distinguish the boundaries. At 1100 °C, the microstructure contains grain boundaries, which are typically related to surface crystallization. Acicular crystals can be observed inside the frit. Intragranular porosity is no longer visible. At 1145 °C, only small crystals are observed at the boundaries of the frits, and the original crystal shapes are no longer apparent.

3.4. Effect of heating rate and holding time

Fig. 9 shows the intensity of the diffraction peaks and the relative density for frit CF as functions of the heating rate and the holding time at 1000 °C. As expected, the longer the holding time, the greater the intensity of the diffraction peak. Peak intensity increased slightly with increasing heating rate. This unexpected effect may be explained by the high surface area due to the material porosity while it passed through the nucleation temperature range at higher heating rates. Thus, there was an increased tendency to form many nuclei on the surface.

Relative densities between 0.93 and 0.96 were found. The increasing relative density from 2 to 10 °C min^{-1} is due to the surface crystallization of the frits. However, the decreasing relative density from 10 to 25 °C min^{-1} may be due to the thermal gradient formed between the surface and the bulk of the sample. This gradient is higher at 25 °C min^{-1}, resulting in greater porosity in the bulk. This effect is more significant when the holding time is decreased. The higher

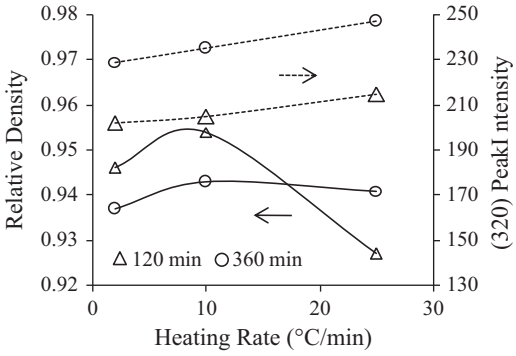

Fig. 9. Relative density and intensity in the crystallographic plane (3 2 0) of wollastonite related to the heating rate and the holding time at 1000 °C for the frit CF.

relative densities observed for 2 and 10 °C min^{-1} at 120 min in relation to 360 min might be caused by the appearance of porosity induced by crystallization. Other authors also observed the reduction of the relative density due to the crystallization of a wollastonite system [14,27].

Fig. 10 shows the microstructure obtained at heating rates of 2 and 25 °C min^{-1}, both for a 360 min holding time. The formation of crystals along the whole sample and certain isolated and rounded pores are visible. The boundary of the frits showed more distinctness for the material obtained at 2 °C min^{-1} due to the longer holding time during the crystallization of wollastonite. This visual effect was observed macroscopically and represents an esthetic effect similar to grains dispersed in a translucent matrix in marble. The same effect can be observed for samples heat treated at 925 and 1100 °C, Fig. 8-e and -g. In the case of the 25 °C min^{-1} heating rate, as well as the 10 °C min^{-1} rate (Fig. 8-f), the lack of distinctness in the boundaries of the frits interfered with the formation of the desired esthetic effect.

Table 3 presents the results for the porosity and the average pore size as functions of the heating rate and the holding time at distinct samples regions. The porosity at the region near the surface is lower than in the bulk with average values of 2.1 and 5.5%, respectively. After a variance analysis (ANOVA), the following results were found: (1) the heating rate has a more significant effect on the porosity near the surface of the frit, i.e., the slower the rate, the lower the porosity; (2) the holding time has a more significant effect on the bulk porosity, i.e., the longer the holding time, the lower the porosity. The relationship between the porosity and the pore size was linear with a correlation coefficient of $R=0.81$.

4. Conclusions

In this paper, the sintering and the crystallization of a glass ceramic material (composition $14.0CaO.5.5Al_2O_3.80.5SiO_2$), as obtained by *Grain Glass Sintering* (*GGS*), were studied with the aim of producing plates with an esthetic effect similar to marbles and granites for use as decorative materials. Using differential thermal analysis (DTA) and heating microscopy, thermal events were correlated with the sintering and the

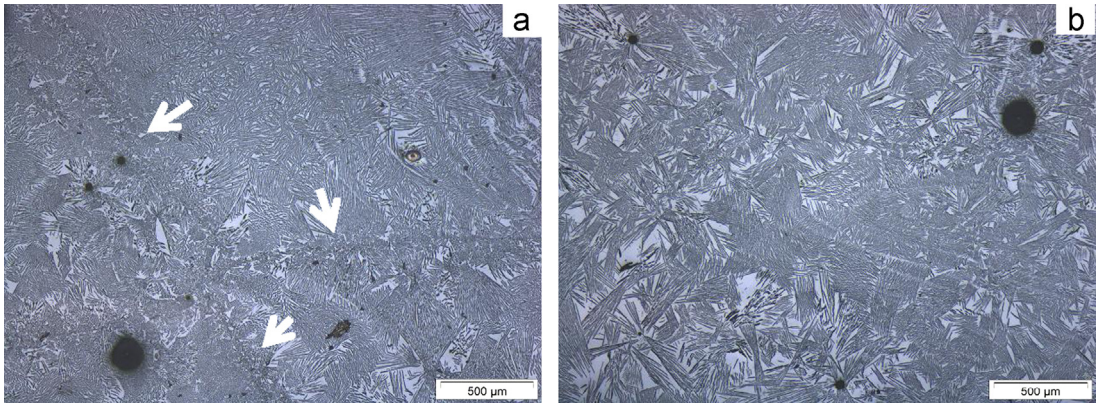

Fig. 10. Micrographs of the samples heat treated at 1000 °C/360 min: (a) 2 °C min^{-1} and (b) 25 °C min^{-1}. Arrows indicate the grain boundaries.

Table 3
Porosity and mean pore size in function of heating rate, holding time, and position at the sample.

Heating rate (°C min^{-1})	**Holding time** (min)	**Position at the sample**	**Mean pore size (μm)**	**Porosity (%)**
2	360	Interior	364	2.1
2	120	Interior	547	5.6
10	360	Interior	274	1.7
10	120	Interior	875	9.8
25	360	Interior	497	5.9
25	120	Interior	748	7.7
2	360	Surface	336	1.3
2	120	Surface	329	0.9
10	360	Surface	544	1.7
10	120	Surface	573	2.1
25	360	Surface	605	3.0
25	120	Surface	597	3.3

crystallization of coarse frits. The maximum sintering temperature increased due to the larger particle sizes in the granular frit. The granular frit underwent more significant sintering than the powder frit, including the temperature of maximum densification rate above the crystallization temperature. Above the crystallization temperature, the intragranular porosity was no longer visible in the microstructure of the material. The premature crystallization of pseudowollastonite was observed and related with the action of some component from the glass that acted as a mineralizing agent. The desired esthetic effect was obtained using coarse frits with crystallization in their boundaries that was capable of generating visual contrast with the particles in the bulk. The esthetic effects change the characteristics of the frits in the range between their crystallization and melting temperatures. A lower heating rate contributed to the visual contrast observed between the boundaries of the frits and the matrix and to the reduction of the superficial porosity. The holding time at the maximum temperature contributed to increasing crystallinity and decreasing bulk porosity in the material.

Acknowledgments

The authors are very grateful to the technicians at the Instituto de Engenharia e Tecnologia (IDT/UNESC) for their technical support and the CNPq (Conselho Nacional de Desenvolvimento Científico e Tecnológico) for their financial support of this research.

References

[1] E. Sanchez, Considerações técnicas sobre Produtos de Revestimentos Porcelânico e seus Processos de Manufatura. Parte I, Ceramic Industries 8 (2003) 1–16.
[2] C. Zanelli, M. Raimondo, G. Guarini, F. Marani, L. Fossa, M. Dondi, Porcelain stoneware large slabs processing and technological properties, Proceedings of XIth World Congress on Ceramic Tile Quality (Qualicer), Castellón (2010) 1–10.
[3] W. Höland, G. Beall, Glass-ceramics Technology, The American Ceramics Society, Westerville, 2002.
[4] V.O. Soares, R.M.C.V. Reis, E.D. Zanotto, M.J. Pascual, A. Duran, Non-isothermal sinter-crystallization of jagged Li_2O–Al_2O_3–SiO_2 glass and simulation using a modified form of the clusters model, Journal of Non-Crystalline Solids 358 (2012) 3234–3242.
[5] F.M. Bertan, O.R.K. Montedo, C. Rambo, D. Hotza, A.P.N. Oliveira, Extruded $ZrSiO_4$ particulate-reinforced LZSA glass ceramics matrix composite, Journal of Materials Processing Technology 209 (2009) 1134–1142.
[6] W.Y. Zhang, H. Gao, Y. Xu, Sintering and reactive crystal growth of diopside-albite glass-ceramics from waste glass, Journal of the European Ceramic Society 31 (2011) 1669–1675.
[7] J. Zhou, Y. Wang, A novel process of preparing glass-ceramics with pseudo-bioclastic texture, Ceramics International 34 (2008) 113–118.

[8] W.Y. Zhang, H. Liu, A low cost route for fabrication of wollastonite glass-ceramics directly using soda-lime waste glass by reactive crystallization-sintering, Ceramics International 39 (2013) 1943–1949.
[9] W.N. Nour, A.A. Mostafa, D.M. Ibrahim, Reclycled wastes as precursor for synthesizing wollastonite, Ceramics International 34 (2008) 101–105.
[10] A. Karamanov, Granite like materials from hazardous wastes obtained by sintercrystallisation of glass frits, Advances in Applied Ceramics 108 (2009) 14–21.
[11] J.E. Shelby, Introduction to Glass Science and Technology. New York State College of Ceramics at Alfred University, The Royal Society of Chemistry, New York, 1997.
[12] J.M.F. Navarro, El Vidrio, third ed., Madrid: Consejo Superior de Investigaciones Cientificas, Madrid, 2003, 684 p.
[13] M.O. Prado, E.D. Zanotto, Glass sintering with concurrent crystallization, Comptes Rendus Chimie 5 (2002) 773–786.
[14] M. Mohammadi, P. Alizadeh, Z. Atlasbaf, Effect of frit size on sintering, crystallization and electrical properties of wollastonite glass-ceramics, Journal of Non-Crystalline Solids 357 (2010) 150–156.
[15] O.R.K. Montedo, F.M. Bertan, R. Piccoli, D. Hotza, A.N. Klein, A.P.N. Oliveira, Low thermal expansion sintered LZSA glass-ceramics, American Ceramic Society Bulletin 87 (2008) 34–40.
[16] O.R.K. Montedo, F.J. Floriano, J. de Oliveira Filho, E. Angioletto, A.M. Bernardin, Sintering behavior of LZSA glass-ceramics, Materials Research 12 (2009) 197–200.
[17] J.M.F. Ferreira, A. Goel, I. Kansal, M.J. Pascual, D.U. Tulyaganov, Structural analysis and thermal behavior of diopside–fluorapatite–wollastonite-based glasses and glass-ceramics, Acta Biomaterialia 6 (2010) 4380–4388.
[18] E.D. Zanotto, Isothermal and adiabatic nucleation in glass, Journal of Non-Crystalline Solids 89 (1987) 361–370.
[19] P.F. James, R.W. Jones, Glass ceramics, in: M. Cable, J.M. Parker (Eds.), High-Performance Glasses, Blackie, New York, 1982, pp. 102–113.
[20] D.U. Tulyaganov, S. Agathopoulos, V.M.F. Marques, J.M.F. Ferreira, Low temperature production of glass ceramics in the anorthite-diopside system via sintering and crystallization of glass powder compacts, Ceramics International 34 (2008) 1145–1152.
[21] B. Philips, A. Muan, Phase equilibrium diagram of the system CaO–SiO_2, Journal of the American Ceramic Society 42 (1959) 414–420.
[22] H.R. Wenk, Polymorphism of wollastonite, Contributions to Mineralogy and Petrology 22 (1969) 238–247.
[23] M. Magallanes-Perdomo, P. Pena, P.N. De Aza, R. Carrodeguas, G.M.A. Rodríguez, X. Turrillas, S. De Aza, A.H. De Aza, Devitrification studies of wollastonite–tricalcium phosphate eutectic glass, Acta Biomaterialia 5 (2009) 3057–3066.
[24] W. Zhang, H. Liu, A low cost route for fabrication of wollastonite glass-ceramics directly using soda-lime waste glass by reactive crystallization-sintering, Ceramics International 39 (2013) 1943–1949.
[25] G.A. Khater, Glass-ceramics in the CaO–MgO–Al_2O_3–SiO_2 system based on industrial waste materials, Journal of Non-Crystalline Solids 356 (2010) 3066–3070.
[26] G. Ottonello, M. Attene, D. Ameglio, D. Belmonte, M. Vetuschi Zuccolini, M. Natali, Thermodynamic investigation of the CaO–Al_2O_3–SiO_2 system at high P and T through polymer chemistry and convex-hull techniques, Chemical Geology 346 (2013) 81–92, http://dx.doi.org/10.1016/j.chemgeo.2012.09.018.
[27] A. Karamanov, M. Pelino, Induced crystallization porosity and properties of sintered diopside and wollastonite glass-ceramics, Journal of the European Ceramic Society 28 (2008) 555–562.